Magnetization Reversal in Ferromagnetic Films Patterned with Antiferromagnetic Gratings of Various Sizes

F. Liu and C. A. Ross

Phys. Rev. Applied **4**, 054005 — Published 18 November 2015

DOI: 10.1103/PhysRevApplied.4.054005

Magnetization Reversal in Ferromagnetic Films patterned with Antiferromagnetic Gratings

Authors: F. Liu, C.A. Ross*
Department of Materials Science and Engineering,
Massachusetts Institute of Technology,
77 Massachusetts Ave, Room 13-4005, Cambridge MA 02139

*caross@mit.edu

Abstract:

The magnetic switching behavior in continuous NiFe films patterned with IrMn gratings was investigated experimentally and with micromagnetic simulations. The samples, made by a two-step deposition process, consisted of a 10 nm thick NiFe layer on which was placed 10 nm thick IrMn stripes with width from 100 nm to 500 nm, and period from 240 nm to 1 μm. Exchange bias was introduced by field-cooling in directions parallel or perpendicular to the IrMn stripes. The samples displayed a two-step hysteresis loop for higher stripe width and period, as the pinned and unpinned regions of the NiFe reversed independently, but a one-step loop for lower stripe periods. The transition between these regimes was reproduced by micromagnetic modeling.

Introduction:

Exchange bias between a ferromagnet (FM) and an antiferromagnet (AFM) is important both in understanding magnetic exchange phenomena and for its applications in devices such as magnetic random access memories and hard disk read heads [1, 2]. Exchange bias leads to a unidirectional anisotropy, a shift of the hysteresis loop and often an increase in coercivity [3,4]. Size effects in exchange-biased FM/AFM bilayers have been studied in several systems in which both layers are deposited sequentially then patterned to have the same lateral dimensions [5-9]. For example, in bilayer FM/AFM stripes consisting of ferromagnetic metals coupled to CoO, NiO, FeMn, or IrMn antiferromagnetic layers, exchange bias along the stripe axis decreased as the stripe width decreased [7, 11, 6, 12] but in another example of NiFe/NiO stripes the exchange bias increased with decreasing stripe width [13].

The magnetic behavior of locally exchange-biased thin films, in which the FM and AFM have different dimensions and the exchange-bias is limited to only part of the FM, differs qualitatively from that of patterned FM/AF bilayers. The reversal mechanism of the FM depends on the length scales of the pinned and unpinned regions and the strength of the exchange bias in the pinned regions. Locally exchange-biased structures

are not only essential for certain domain-wall memory or logic devices [14, 11], but also provide insights into exchange bias phenomena [15, 16]. For example, continuous NiFe films with overlaid FeMn stripes of μm-scale period showed asymmetrical hysteresis loops [17, 18] suggesting the pinned and unpinned regions reverse at different fields. Exchange bias parallel to the stripes produced switching in two steps, whereas exchange bias perpendicular to the stripes produced switching in one step [19]. Understanding and manipulating the reversal process of a magnetic film with local exchange bias is therefore a key part of magnetic device design, providing for example the ability to trap a domain wall or to initiate reversal in a magnetic nanostructure, but despite its importance, the behavior of magnetic films patterned with submicron antiferromagnetic features and how the regions interact at smaller dimensions has not been explored.

This study analyzes the switching behavior of NiFe continuous films patterned with stripes of IrMn as a function of both the period and width of the IrMn stripes. The structures are made by a two step deposition process and subsequently field-cooled. Phase maps describe the reversal process as a function of pattern geometry and the results are compared to micromagnetic predictions. The results show the interplay between interface exchange bias and the exchange coupling within the bulk of the NiFe film in determining the hysteresis behavior.

Magnetic films with local exchange bias can be prepared subtractively, i.e. the removal of regions of the AF from an AF/FM bilayer. This can be accomplished by ion beam etching [17], but this is a non-selective etch which can also damage the FM [20]. Ion bombardment of an AF/FM bilayer through a resist mask can locally alter magnetic properties [18, 15, 16], for example, by oxidizing an AFM in select portions of the film [19]. However, the lateral resolution of this technique is limited by ion straggle and it has been limited to introducing exchange bias into features larger than 1μm. Alternatively, additive methods have been developed, such as the deposition of FM nanodots onto a continuous AFM layer through a porous membrane used as a shadow mask [7]. However, contamination of the AF/FM interface between the two separate deposition steps can degrade the exchange bias. To improve the interface coupling, we previously presented a hybrid method [21] in which a pre-deposited NiFe film was etched back by 1 nm to remove any surface oxides, followed by growth of 1 nm additional NiFe then an IrMn film. This produced exchange bias similar to that found in NiFe/IrMn grown without a vacuum break.

Methods:

The patterned samples were prepared using a modification of a process presented earlier [21]. Ta (5 nm)/$Ni_{80}Fe_{20}$ (10 nm) was deposited on top of a Si wafer using triode

sputtering at 2×10^{-8} Torr base pressure and 1 mTorr Ar pressure with a growth rate of 0.132 nm/s. A grating pattern mask was then fabricated on the NiFe using interference lithography [22]. A tri-layer stack of antireflective coating (ARC) (315 nm) / SiO_2 (20 nm) / PS4 negative resist (Ohka) (215 nm) was first deposited as shown in the schematic in Figure 1. The thickness of the ARC was chosen to minimize reflections of the laser from the substrate to prevent vertical standing waves. The ARC layer was made by spin coating and baking, then the silica layer by electron beam evaporation, and a thin layer of hexamethyldisilazane was spun to promote adhesion of the PS4 resist onto the silica. The PS4 resist was spun at 3 krpm and baked at $90°$ C for 90 s. The resist was then exposed to two beams from a 325 nm wavelength HeCd laser source whose interference produced a grating pattern exposure with periodicity of 240 nm – 1 μm. The resist was then developed and a two-step RIE process was performed to transfer the pattern into the ARC: CF_4 to etch the SiO_2 and then O_2 to etch the ARC to form a grating. Figure 1b shows a scanning electron microscope (SEM) image of the resulting mask.

The samples were then ion beam etched for 3s (Ar pressure 2×10^{-4} Torr, beam current 5.5 mA, voltage 500V, etch rate 0.256 nm s^{-1}) to clean the exposed surface of the NiFe. A 1 nm layer of NiFe was then deposited followed by IrMn (10 nm) deposited at 1 mTorr Ar pressure at a rate of 0.2 nm s^{-1}, then a layer of Ta (5 nm) to prevent oxidation of the magnetic layers. Lastly, the remaining ARC stack was lifted off using N-methyl-2-pyrrolidone (NMP). A SEM image of the final structure is shown in Figure 1c. This results in a film of NiFe exchange-coupled to overlaid stripes of IrMn. The IrMn stripe periodicity varied from 240 nm to 1 μm while the stripe width varied from 100 nm to 500 nm. Unpatterned control samples of IrMn/NiFe were also made for comparison. The interference lithography process produced samples of area 5 x 5 mm^2 with large enough magnetic moment to be measurable using vibrating sample magnetometry (VSM) (ADE model 1660) at room temperature.

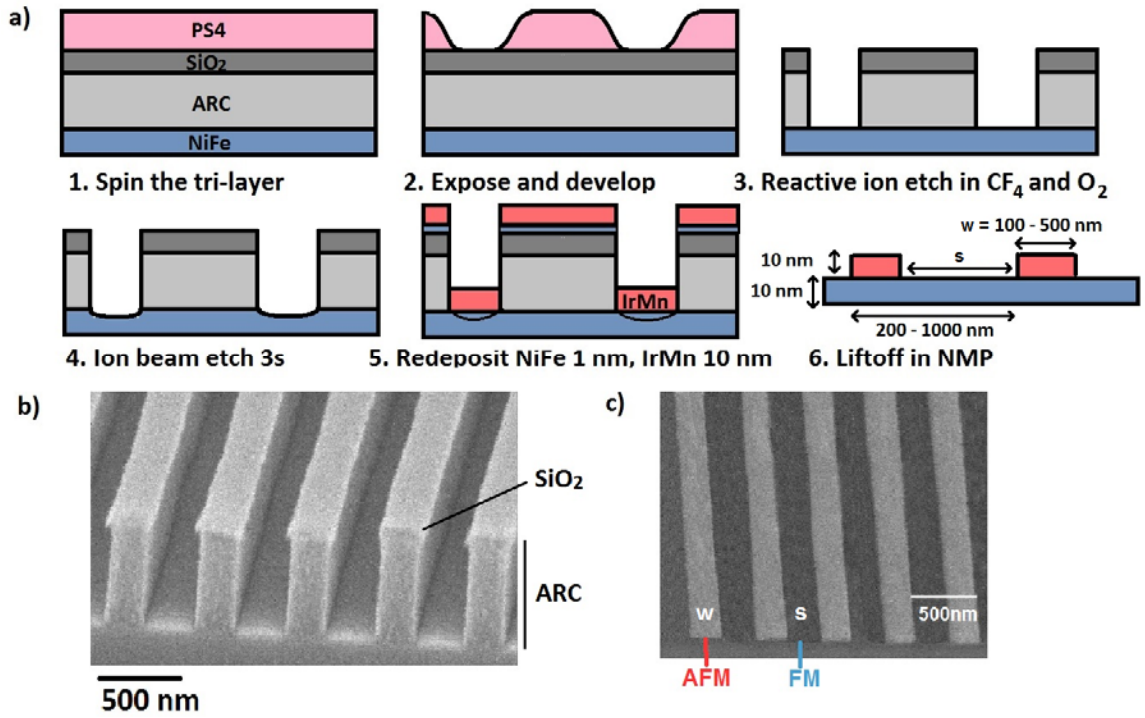

Figure 1. a) Schematic of the sample fabrication procedure. In steps 1-3 the resist mask is made; in steps 4-6 the AFM is patterned. b) SEM image of a resist mask with period 500 nm. c) SEM image of a patterned sample with period 500 nm showing IrMn stripes of width w separated by regions of unbiased NiFe of width s.

To exclude effects from the ion beam etch on the magnetic properties of the NiFe, the hysteresis loop of an as-grown 10 nm NiFe film was compared with a 10 nm NiFe film that had been subjected to 3s of ion beam etching, followed by redeposition of 1 nm NiFe. The loops were measured to 1000 Oe range, with increments of 1 Oe near the switching field. The films had the same coercivity, switching field, and magnetization to within the resolution of the measurement.

The exchange bias was initially set by field-cooling at 10 kOe from a temperature of 520 K. The exchange bias was set either parallel to the IrMn stripes, or in-plane perpendicular to the IrMn stripes. Due to significant training effects [23], as seen in NiFe/IrMn dots [21], the samples were field-cooled from 550 K after each hysteresis measurement.

The object-oriented micromagnetic framework (OOMMF) package [24] was used to model the switching behavior as a function of IrMn stripe width and spacing. The OOMMF timedriver is based on the Landau-Lifshitz-Gilbert equation [25], $\frac{dM}{dt} = -\gamma\left(M \times H_{eff} - \alpha \frac{M}{M_s} \times \frac{dM}{dt}\right)$, where γ is the electron gyromagnetic ratio, M is the

magnetization, H_{eff} is the effective field which includes the external magnetic field and the demagnetizing field, and α is the damping factor. A damping factor of 0.5 was used in these simulations for fast convergence. A saturation of 800 Oe, exchange energy of 13×10^{-5} erg, and an anisotropy energy of 8000 erg/cm^3 were used [24]. The cell size was 5 nm x 5 nm x 5 nm, as used in prior simulations of NiFe [24] and consistent with the exchange length of NiFe (~5.7 nm) [26]. The simulation size in the direction parallel to the stripes was 2 μm to minimize the influence of edge effects. The exchange bias was modeled as a fixed external field present in the regions of NiFe covered with the IrMn stripes. This is a simplification of the exchange bias, which affects only the NiFe at the NiFe/IrMn interface, but was justified here because the film thickness corresponded to only two layers of cells which had almost identical magnetization directions. Periodic boundary conditions in the in-plane direction perpendicular to the stripes were used to model an infinite stripe array.

Results and discussion

A. Exchange bias parallel to grating

We first discuss in Fig. 2 the experimental results for samples with exchange bias and applied field parallel to the stripes, with *s* (the width of the unbiased regions of NiFe) and *w* (the width of the biased regions of NiFe) in the range of 100 nm to 500 nm. At small *w* and *s*, the hysteresis loops showed a single step (Fig. 2b), but as the dimensions increased the loops showed two steps attributed to the switching of the pinned and unpinned regions of the film (Fig. 2c-e). The criterion to identify a two-step reversal was the existence of a kink or plateau on at least one branch of the hysteresis loop occurring at a magnetic moment close to the value expected from the relative widths *w* and *s* of the stripes. In some cases the plateau was only evident on one branch of the hysteresis loop, as in Fig. 2c, because on the other branch the offset of the loop due to exchange bias was counteracted by an increase in coercivity.

The type of hysteresis loop of all the samples was plotted on a phase diagram, Figure 2a, showing a region of one-step reversal for values of *w* and *s* below 300 nm, i.e. for these dimensions the pinned and unpinned regions reverse within a few Oe of each other.

In the samples that showed two-step reversal we would expect the magnetization at the plateau to be simply related to the ratio of *s* and *w*. For example in Figure 2c, the geometry of the sample (*w* = 200 nm, *s* = 300 nm) suggests the first step of the descending branch of the hysteresis loop would correspond to 0.6 of the total change in magnetization. However, the measured step height was 0.67, i.e. the effective width of the pinned region was 167 nm. This is consistent with part of the pinned region, in this case 17 nm, reversing with the unpinned region due to exchange coupling in the NiFe film. Samples with other dimensions showed similar results with the effective width of the unpinned region given by the nominal width plus 15 nm ± 2 nm.

Fig. 3 shows the trends in coercivity and exchange bias with pattern dimensions. The coercivity of two-step loops is defined as the field at which the unpinned region magnetization reversed, measured half way up the step. The coercivity increased from 60 Oe to 150 Oe as *s* decreased, but there was no systematic variation with *w*. The coercivity of unpatterned NiFe/IrMn samples varied from 100 Oe to 170 Oe.

The exchange bias was 25 – 70 Oe. As a comparison, unpatterned NiFe/IrMn bilayer films showed exchange bias of 80 – 120 Oe. A reduction of exchange bias in patterned structures compared to continuous bilayers is consistent with other studies [27, 28]. The exchange bias increased slowly with *s*. It showed little variation for 100 nm $\leq w \leq$ 350 nm but was larger for w = 500 nm. Prior work has shown [3] that a reduction of feature size can cause an increase, decrease, or no change in the exchange bias. The magnitude of the exchange bias has been associated with the AFM domain size [28], which is limited by the size of the features in patterned samples. In our system, the 10 nm thick IrMn is expected to have a domain size of ~320 nm [28], wider than the narrowest values of *w*, suggesting that exchange bias would increase with decreasing *w*. On the other hand, features with narrower *w* are more vulnerable to thermal instability of the moments near the edges of the structures [12].

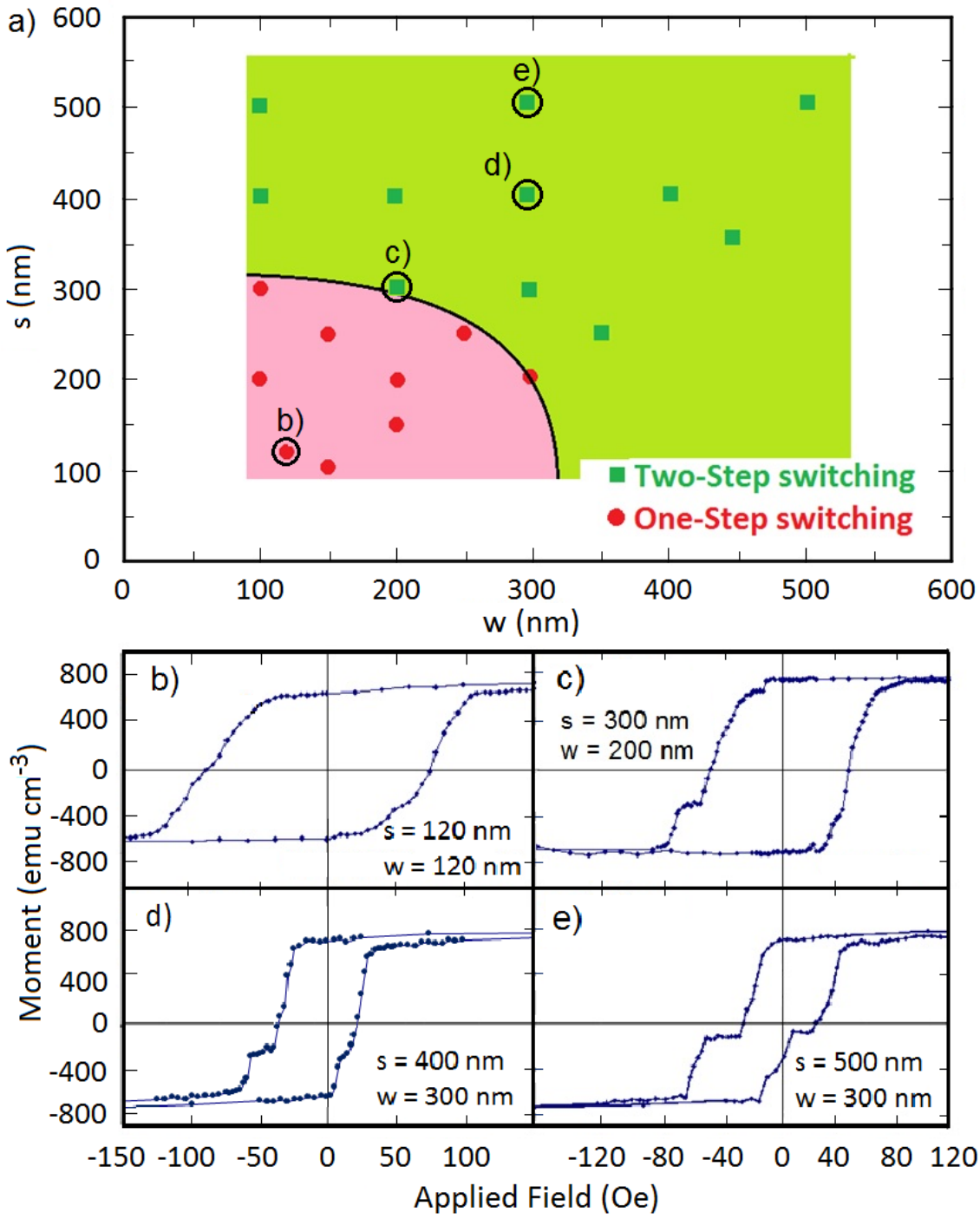

Figure 2. a) Experimental phase diagram of the switching behavior. b) An example of one-step switching, for s = w = 120 nm. Example loops for two-step switching: c) s = 300 nm, w = 200 nm. d) s = 400 nm, w = 300 nm; e) s = 500 nm, w = 300 nm.

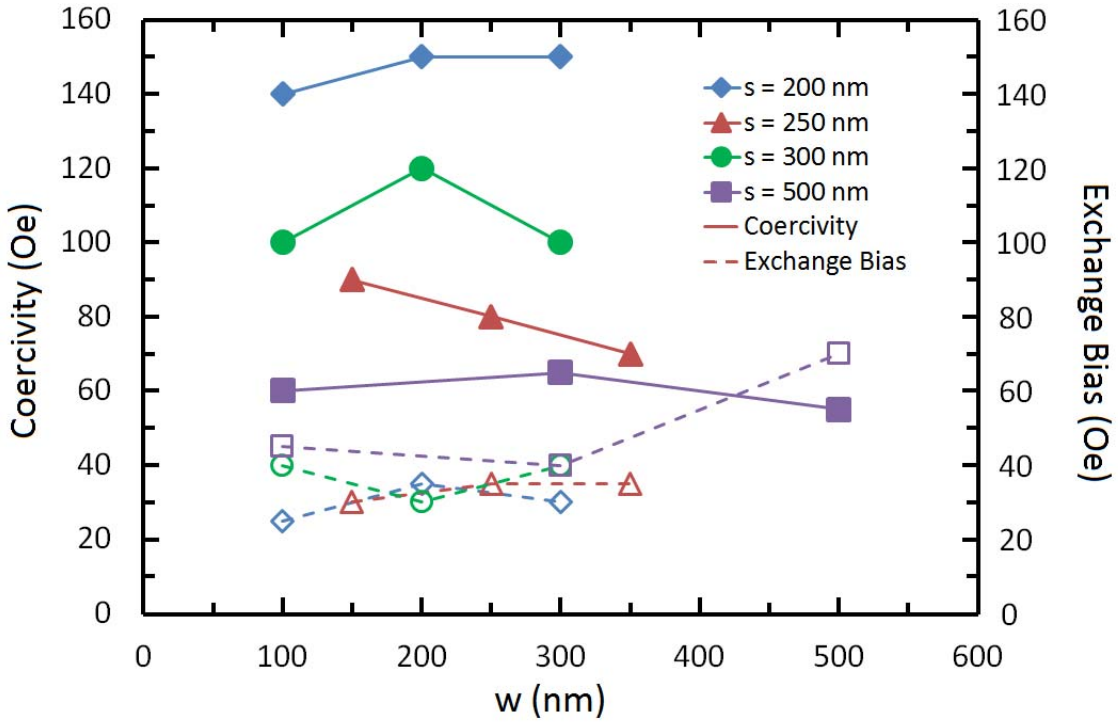

Figure 3. Measured exchange bias and coercivity versus IrMn stripe width w for four different values of s. For samples that show two step switching, the coercivity is for the unpinned region.

To interpret the results, micromagnetic simulations were performed with the magnetic field and the exchange bias of 100 Oe both parallel to the stripe length *y*, Fig. 4. The schematic in Figure 4a shows a unit cell used in the simulation. Each data point in the modeled hysteresis loops indicates the magnetization along *y* calculated after initializing the moments to random directions then allowing them to relax in the corresponding applied field. This method was used to produce ground state magnetization configurations as a function of field. Calculations in which the magnetic configuration was allowed to evolve as a function of field without reinitializing at each field step led to very high switching fields due to the high symmetry and the periodic boundary conditions, trapping metastable configurations. This was the case even when notches, a field offset of 2˚, or a spread in magnetic anisotropy between cells was introduced.

Examples are shown in Fig. 4(b-e) for several combinations of *w* and *s*. For smaller dimensions, the magnetization in the relaxed state was aligned along either +*y* or –*y* with high remanence (Fig. 4(b)), but for larger dimensions, a limited range of fields produced a state in which the magnetization of the pinned and unpinned regions of the NiFe was antiparallel and the net magnetization took an intermediate value (Figs. 4(c-e)). These cases represent one-step and two-step reversal, respectively. Figure 4(a) shows a phase diagram that summarizes the results as a function of *s* and *w*. The phase boundary

between one-step and two-step reversal is labeled as T_1, and resembles the experimental results, Fig. 2(a). For two-step reversal, the value of magnetization at the plateau was field dependent, showing that the width of the reversed region did not simply correspond to the width of the unpinned region but increased with increasing field.

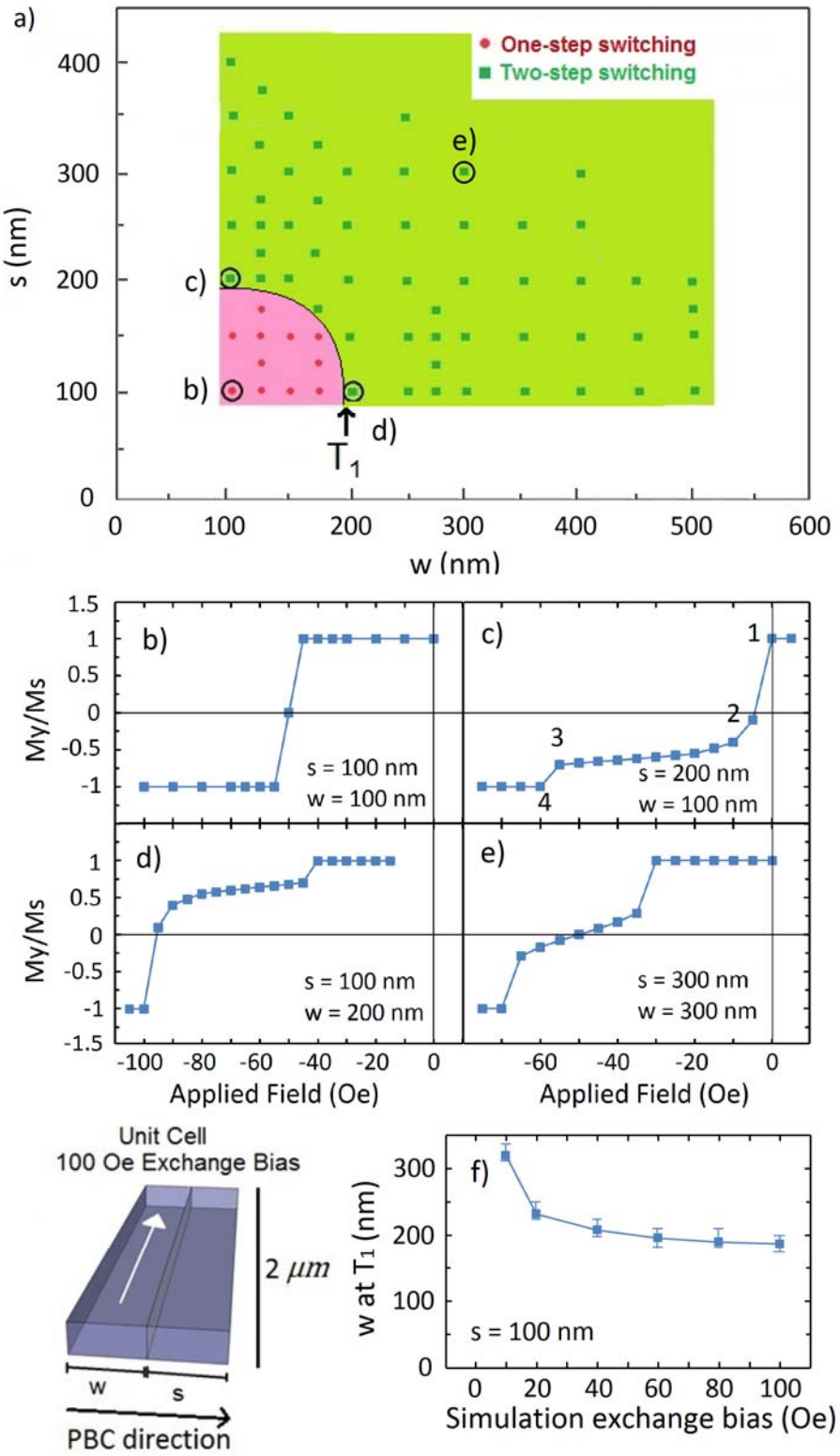

Figure 4. a) Phase diagram for switching behavior of the patterned structure with both exchange bias and applied field parallel to the stripe length. T_1 indicates the phase boundary. b) An example of one-step switching, and (c,d,e) examples of two-step

switching. The dimensions correspond with the points labelled (b-e) in the phase diagram. The numbers in the hysteresis loop (c) refer to the micromagnetic images in Figure 4. (f) The values of w for s =200 nm at the transition T_1 as a function of exchange bias.

The reversal process can be seen in more detail from the micromagnetic configurations vs. field. Figure 5 shows an example from the descending branch loop of Fig. 4(c) (w = 100 nm, s = 200 nm) with positive magnetization direction in red and negative in blue. The unpinned region, as well as 14 nm width of the pinned region, had reversed in panel 2 at -5 Oe field. This distance is about twice the exchange length of NiFe (~5.7 nm) [26]. Similar behavior was seen for other model geometries exhibiting 2-step loops. As the reverse field increased to -55 Oe, panel 3, the pinned region gradually reversed from the edges and reduced in width, with reversal completed at -60 Oe, panel 4. In contrast, complementary behavior was seen in simulations with $w > s$ (Fig. 4(d) (w = 200 nm, s = 100 nm). At the switching field of -45 Oe, only the center part of the unpinned region switched. Increasing negative fields led to a gradual expansion of the reversed region and reversal was complete at -100 Oe.

The pinning is simply modeled as a region subject to a different effective field. During the reversal, exchange coupling caused part of the narrower region to switch with the wider region. In the case of $w = s$, increasing negative field first reversed the center of the unpinned region which expanded into the pinned region as the field increased, and the midpoint of the plateau corresponded to zero net magnetization, Fig. 4(b, e).

In contrast, for combinations of s and w within boundary T_1, both pinned and unpinned regions reversed together without the formation of 180˚ walls. As the exchange bias in the model was decreased, T_1 moved to larger values of w and s. Fig. 4(f) shows the change in T_1 with exchange bias. For example, when s = 200 nm, T_1 occured at w = 100 nm for 100 Oe exchange bias and at w = 150 nm for 40 Oe exchange bias.

The model therefore shows that one-step switching is promoted at lower stripe dimensions both by the increased energetic cost per unit area of forming the 180˚ domain walls, and by the reduction in exchange bias in structures with lower dimensions. The agreement with the experiment is quite good considering the simplifications of the model, which include zero temperature, periodic boundary conditions in only one direction, and the treatment of exchange bias as a fixed Zeeman field in the film. More realistic treatment of exchange bias, such as modeling the AF as a fraction of pinned and rotatable magnetic cells representing uncompensated moments [29], may produce better quantitative agreement with the experimental observations.

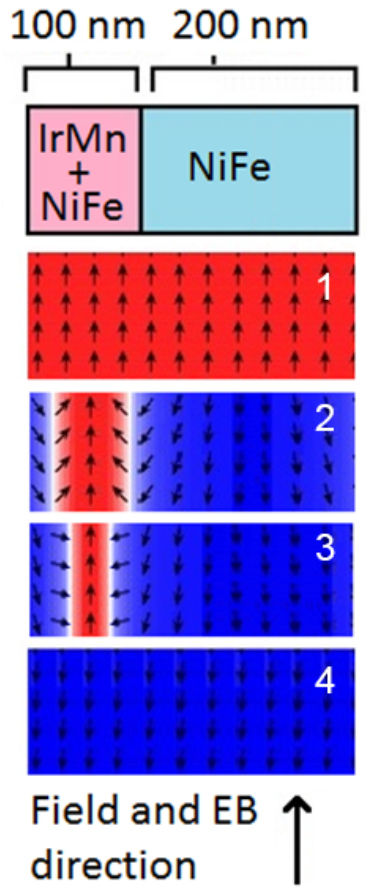

Figure 5. OOMMF micromagnetic images under fields corresponding to Figure 3(c), for s = 200 nm, w = 100 nm. Panels 1, 2, 3, 4 depicts the equilibrium configuration at 0 Oe, -5 Oe, -55 Oe and -60 Oe.

B. Exchange bias perpendicular to grating

When the field cooling and in-plane applied field were perpendicular to the stripe length, two-step switching was observed in samples with larger *w* and *s*, summarized in the phase diagram in Figure 6(a). The boundary T_2 between one-step and two-step switching regimes occurred at higher *w* and *s* compared with T_1 described above for samples with exchange bias parallel to the lines. Moreover, the measured exchange bias in the two-step loops was 20 to 35 Oe, lower than for the parallel case (25 to 50 Oe). This result differs from a study of wider stripes [20], which observed no two-step switching, even up to 20 μm periodicity.

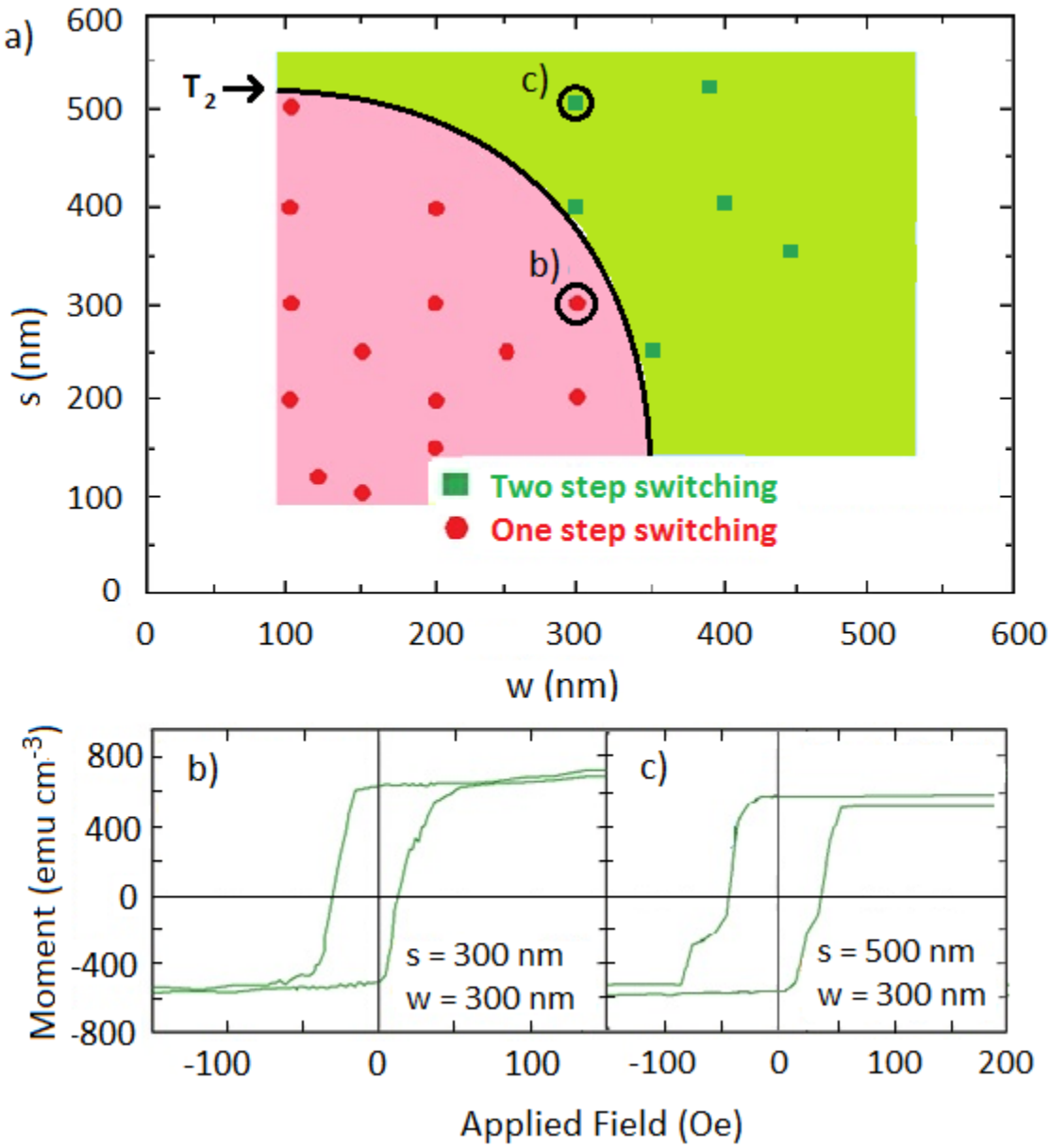

Figure 6. a) Experimental phase diagram of the switching behavior in the samples exchange biased and measured perpendicular to the wire length. b) An example loop for one-step switching. c) An example loop for two-step switching.

The simulations, however, predicted one-step switching for all combinations of *w* and *s* tested in the range of 100 nm to 500 nm, Figure 7(a). This result was obtained for hysteresis loops calculated with no offset or with a 1° offset between the applied field and the direction transverse to the lines in order to break the symmetry of the simulation, and also for relaxation from a random magnetization state. Images of the equilibrium magnetic configuration are shown at fields of -170 Oe and -180 Oe, just below and just above the switching field, Fig. 7(c,d), as well as a dynamic intermediate state calculated

from the state at (c) by applying a field of -180 Oe with damping parameter $\alpha = 0.01$. The switching proceeded incoherently with the unpinned region reversing first, producing a head-to-head 180˚ domain wall.

A larger simulation with an increased exchange bias of 1000 Oe and $s = w = 2000$ nm did produce two step switching, which shows that for sufficiently large exchange bias and wire widths, two step switching can take place. However, for the smaller dimensions and lower exchange bias in Fig. 7(a) the energetic cost of the head-to-head 180˚ domain walls, which have greater stray field and greater width than the walls formed when the exchange bias and field are parallel to the stripes, preclude two step reversal in the model.

In comparison, 30 nm NiFe patterned with 2 – 20 μm IrMn stripes [19] showed only single step reversal for exchange bias and field perpendicular to the stripes. The lack of two step switching was attributed to the interstripe extension of domain walls and overlapping tails of the Néel walls. Furthermore, the greater thickness of the NiFe (and hence the domain wall size) and the modest exchange bias values (a few Oersteds) would promote single-step switching behavior at much larger stripe dimensions.

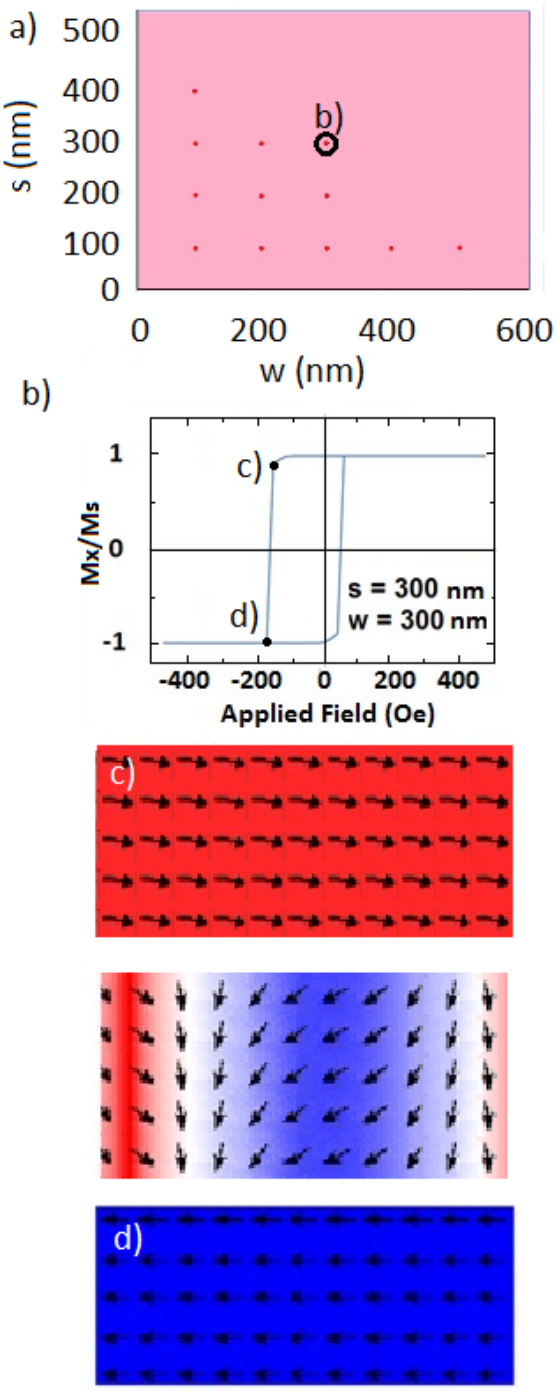

Figure 7. a) Phase diagram for switching behavior of the patterned structure with exchange bias in-plane along x, perpendicular to the wire length. All the modeled dimensions resulted in one-step switching. b) Example of a loop showing one-step switching. Magnetic configurations are shown at 170 Oe before the switch (c), and at 180 Oe after the switch (d), along with an intermediate state calculated dynamically by applying a field of 180 Oe to (c). The figures represent 600 nm width.

Summary

Local exchange bias was obtained in continuous 10 nm thick NiFe films overlaid with arrays of 10 nm thick IrMn stripes. The samples were fabricated using interference lithography combined with an etch and sputter deposition process to yield stripe widths of 100 – 500 nm and periods of 240 – 900 nm. The magnetic switching behavior was mapped out as a function of dimensions both experimentally and by micromagnetic modeling. In the patterned samples, at low wire widths and spacings, the pinned and free regions switched together, but as the width and spacing of the wires increased, the pinned and unpinned regions reversed at different fields giving a two step loop. Micromagnetic modeling provided insight into the reversal process, reproducing the change in reversal process with stripe width for exchange bias and field parallel to the stripes. However, the simulations predicted single step reversal for exchange bias and field perpendicular to the stripes unless the exchange bias and period were large, which disagreed with the experiments.

Although the fabrication method and magnetic properties were demonstrated for a continuous film of NiFe, these results can be extended to structures in which the FM layer is also patterned, such as magnetic memory devices consisting of magnetic wires with AF pads at the ends, [14] or to exchange-biased materials with perpendicular anisotropy. These results demonstrate the effect of pattern dimensions on the magnetic properties and reversal mechanisms of locally exchange biased thin films.

Acknowledgements

The authors gratefully acknowledge the support of the National Science Foundation and C-SPIN, a STARnet Center of the Semiconductor Research Corporation supported by DARPA and MARCO. Facilities of the MIT Center for Materials Science and Engineering (NSF DMR1419807) and the NanoStructures Laboratory were used. We thank Jim Daley for his assistance with electron-beam evaporation and Dr Tim Savas for his advice on interference lithography.

References:

[1] V. Baltz, J. Sort, B. Rodmacq, B. Dieny, and S. Landis, Size effects on exchange bias in sub-100 nm ferromagnetic–antiferromagnetic dots deposited on prepatterned substrates, Appl. Phys. Lett. **84**, 4923 (2004)

[2] A. Hoffmann, M. Grimsditch, J. E. Pearson, J. Nogues, W. A. A. Macedo, and I. K. Schuller, Tailoring the exchange bias via shape anisotropy in ferromagnetic/antiferromagnetic exchange-coupled systems, Phys. Rev. B **67**, 220406 (2003)

[3] J. Nogues, J. Sort, V. Langlais, V. Skumryev, S. Surinach, J.S. Munoz, and M.D. Baro, Exchange bias in nanostructures, Phys Rep. **422,** 65 (2005)

[4] J. Nogues and I.K. Schuller, Exchange bias, J Magn. Magn. Mater. **192**, 203 (1999)

[5] Z.P. Li, O. Petracic, J. Eisenmenger, and I.K. Schuller, Reversal behavior of exchange-biased submicron dots, Appl. Phys. Lett. **86,** 072501 (2005).

[6] Y. Shen,Y.Wu, H. Xie, K. Li, J. Qiu, and Z. Guo, Exchange bias of patterned NiFe/IrMn film, J. Appl. Phys. **91,** 8001 (2002)

[7] K. Liu, J. Nogues, C. Leighton, H. Masuda, K. Nishio, I.V. Roshchin, and I.K. Schuller, Fabrication and thermal stability of arrays of Fe nanodots, Appl. Phys. Lett. **81,** 4434 (2002)

[8] J.Yu, A.D. Kent, and S.S.P. Parkin, Exchange biasing in polycrystalline thin film microstructures, J. Appl. Phys. **87,** 5049 (2000)

[9] E. Girgis, R.D. Portugal, M.J. Van Bael, K. Temst, and C. Van Haesendonck, Asymmetric magnetization reversal in exchange-biased NiFe/ CoO submicron-sized structures, J. Appl. Phys. **97,** 103911 (2005)

[10] S.H. Chung, A. Hoffmann, and M. Grimsditch, Interplay between exchange bias and uniaxial anisotropy in a ferromagnetic/antiferromagnetic exchange-coupled system, Phys. Rev. B **71**, 214430 (2005)

[11] D.M. Bromberg, D.H. Morris, L. Pileggi, and J. Zhu, Novel STT-MTJ device enabling all-metallic logic circuits, IEEE Trans. Mag. **48**, 11, 3215 (2012)

[12] M. Fraune, U. Rudiger, G. Guntherodt, C. Cardoso, and P. Freitas, Size dependence of the exchange bias field in NiO/Ni nanostructures, Appl. Phys. Lett. **77,** 3815 (2000).

[13] A. Nemoto,Y. Otani, S.G. Kim, K. Fukamichi, O. Kitakami, and Y. Shimada, Magnetoresistance and planar Hall effects in submicron exchange-coupled NiO/Fe19Ni81 wires, Appl. Phys. Lett. **74,** 4026 (1999).

[14] J.A. Currivan, Y. Jang, M.D. Mascaro, M.A. Baldo, and C.A. Ross, Low energy magnetic domain wall Logic in short, narrow, ferromagnetic wires, IEEE Magn. Lett, **3**, 3000104 (2012)

[15] J. Fassbender and J. McCord, Magnetic patterning by means of ion irradiation and implantation, J. Magn. Magn. Mater. **320**, 579 (2008)

[16] J. McCord, L. Schultz, and J. Fassbender, Hybrid Soft-Magnetic Lateral Exchange Spring Films Prepared by Ion Irradiation, Adv. Mater. Weinheim, Ger. **20**, 2090 (2008)

[17] Z.B. Guo, K.B. Li, G.C. Han, Z.Y. Liu, P. Luo, and Y.H.Wu, Exchange bias in patterned FeMn/NiFe bilayers, J. Magn. Magn. Mater. **251,** 323 (2002).
[18] C. Hamann, J. McCord, L. Schultz, B.P. Toperverg, K. Theis-Bröhl, M. Wolff, R. Kaltofen, and I. Mönch, Competing magnetic interactions in exchange-bias-modulated films, Phys. Rev. B, **81**, 024420 (2010)
[19] C. Hamann, I. Monch, R. Kaltofen, R. Schafer, T. Gemming, L. Schultz, and J. McCord, Size effects on the magnetization reversal behavior of exchange bias modulated thin films, J. Appl. Phys, **104**, 013926 (2008)
[20] A. Scherer, H. G. Craighead, M. L. Roukes, and J. P. Harbison, Electrical damage induced by ion beam etching of GaAs, J. Vac. Sci. Techol. B **6**, 277 (1988)
[21] F. Liu and C.A. Ross, Size-dependent magnetic properties of 100–500 nm diameter IrMn/NiFe disks made by a two-step deposition process, J. Appl. Phys. **116**, 194307 (2014)
[22] A. Gombert, B. Bläsi, Ch. Bühler, P. Nitz, J. Mick, W. Hoßfeld, and M. Niggemann, Some application cases and related manufacturing techniques for optically functional microstructures on large areas, Opt. Eng., **43**, 11, 2525 (2004)
[23] C. Binek, S. Polisetty, X. He, and A. Berger, Exchange bias training effect in coupled all ferromagnetic bilayer structures, Phys. Rev. Lett, **96**, 067201 (2006)
[24] M Donahue, D Porter - URL: http://math. nist. gov/oommf, (1998)
[25] T.L. Gilbert, A phenomenological theory of damping in ferromagnetic materials, IEEE Trans. Mag. **40**, 6, 3443 (2004)
[26] G.S. Abo, Y. Hong, J. Park, J. Lee, W. Lee, and B. Choi, Definition of magnetic exchange length, IEEE Trans. Mag. **49**, 8, 4937-4939 (2013)
[27] J. I. Martin, J. Nogués, K. Liu, J. L. Vicent, and I. K. Schuller, Ordered magnetic nanostructures: fabrication and properties, J. Magn. Magn. Mater. **256**, 449 (2003)
[28] V. Baltz, J. Sort, S. Landis, B. Rodmacq, and B. Dieny, Tailoring size effects on the exchange bias in ferromagnetic-antiferromagnetic< 100 nm nanostructures, Phys. Rev. Lett. **94,** 117201 (2005)
[29] D.A. Gilbert, L.Ye, A. Varea, S. Agramunt-Puig, N. del Valle, C. Navau, J.F. López-Barbera, K.S. Buchanan, A. Hoffmann, A. Sánchez, J. Sort, K. Liu and J. Nogués, A new reversal mode in exchange coupled antiferromagnetic/ferromagnetic disks: distorted viscous vortex, Nanoscale, **7**, 9878 (2015)